Lipid-Protein Interactions are Unique Fingerprints for Membrane Proteins

Valentina Corradi,[†] Eduardo Mendez-Villuendas,[†] Helgi I. Ingólfsson,[‡] Ruo-Xu Gu,[†] Iwona Siuda,[†] Manuel N. Melo,[‡] Anastassiia Moussatova,[†] Lucien J. DeGagné,[†] Besian I. Sejdiu,[†] Gurpreet Singh,[†] Tsjerk A. Wassenaar,[‡] Karelia Delgado Magnero,[†] Siewert J. Marrink[‡], D. Peter Tieleman[†,]*

† Centre for Molecular Simulation and Department of Biological Sciences, University of Calgary, 2500 University Drive NW, Calgary, AB, Canada T2N 1N4

‡ Groningen Biomolecular Sciences and Biotechnology Institute and Zernike Institute for Advanced Materials, University of Groningen, Nijenborgh 7, 9747 AG Groningen, The Netherlands

SUPPORTING INFORMATION

Methods

Systems Setup. The starting structure of each protein, after removal of all the non-protein molecules, was converted in a CG model using the martinize protocol as described on Martini website (http://www.cgmartini.nl/), choosing the option of applying an elastic network on atom pairs within a 0.9 nm cut-off. One elastic network was applied when multiple chains were present, with the exception of AQP1, for which separate elastic networks were applied, one for each monomer of the tetramer. In the case of P-gp, the distance cut-off for the elastic network was increased to 1.0 nm, in order to include few elastic bonds between the two cytosolic domains. The initial simulation setup for GluA2 did not include the elastic network, which was added after 38 μs of simulation time, for additional 10 μs.

For each protein, the transmembrane region was identified using the corresponding entry of the OPM database.[1] Four copies of each CG protein were placed in a simulation box of ca. 42x42 nm in x and y, and lipids, in a composition corresponding to the plasma membrane model developed by Ingólfsson and colleagues,[2] were added using *insane*,[3] for a total of ca. 6000 lipid molecules in each system. Overall, the following lipid classes were included: Cholesterol (CHOL), in both leaflet; charged lipids phosphatidylserine (PS), phosphatidic acid (PA), phosphatidylinositol (PI), and the PI-phosphate, -bisphosphate, and -trisphosphate (PIPs) were placed in the inner leaflet, and ganglioside (GM) in the outer leaflet. The zwitterionic phosphatidylcholine (PC), phosphatidylethanolamine (PE), and sphingomyelin (SM) lipids were placed in both leaflets, with PC and SM primarily in the outer leaflet and PE in the inner leaflet. Ceramide (CER), diacylglycerol (DAG), and lysophosphatidylcholine (LPC) lipids were also included, with all the LPC in the inner leaflet and CER, and DAG primarily in the outer leaflet.[2]

The exact lipid composition of each system is given in Supporting_Information_File_1.xlsx. Water molecules, counterions and 150 mM NaCl were also added.

Simulation Setup. Simulations were performed using the GROMACS simulation package version 4.6.3,[4] with the standard Martini v2.2 simulation settings.[5] After initial energy minimization with position restraints applied on the protein beads (using a force constant of 1000 kJ mol^{-1} nm^{-2}), short equilibrium runs were performed first with the position restraints applied to all the protein beads, and then to the backbone beads. All simulations were performed with a 20 fs time step, a temperature of 310 K set using a velocity-rescaling thermostat,[6] with a time constant for coupling of 1 ps (2 ps for equilibrium runs). A semi-isotropic pressure of 1 bar maintained with the Berendsen barostat,[7] with a compressibility of $3 \cdot 10^{-4}$ $bar^{-1,}$ and a relaxation time constant of 5 ps. Production runs of the duration of 30 μs were performed in the presence of position restraints applied to the backbone beads, with a force constant of 1 1000 kJ mol^{-1} nm^{-2}. DAT and GLUT1 were simulated with the presence of position restraints on the PO4 beads of selected phospholipids (POPC and PIPC in the upper leaflet), as in Ingolfsson et al.[2] All the analyses, unless otherwise specified, were performed on the last 5 μs of each simulation system.

Additional simulations or extended simulations were carried out for the following systems. The simulation for Kv1.2 was extended to 50 μs. For AQP1, we extended the production run to 50 μs and the following additional simulations were performed: (i) 50 μs simulation with no position restraints on the backbone beads and with position restraints on the PO4 beads of PIPC and POPC lipids in the upper leaflet, as in ref. [2] (Setup 2 in Supporting_Information_File_2.xlsx); (ii) 50 μs simulation with no position restraints on the backbone beads and no glycolipids in the system (Setup 3 in Supporting_Information_File_2.xlsx); (iii) as Setup 2 but with polarizable

water model,[8] (Setup 4, in Supporting_Information_File_2.xlsx). For Na,K-ATPase, after the 30 μs long simulation performed with position restraints on the backbone, the glycolipids were removed from the membrane, and the system was simulated for additional 20 μs (Setup 5 in Supporting_Information_File_2.xlsx).

Analyses. For the analyses below, lipids are categorized based on the head group type (PC, PE, PS, PA, DAG, LPC, SM, CER, PI, PIPs, GM) or tails properties. For the tails, we define four classes, as in Ingolfsson et al.[2]: fully-saturated (FS), poly-unsaturated (PU), cholesterol (CHOL) and Others, with the last group defining lipids not present in the first three groups. The PU lipid class consists of DAPC, DUPE, DAPE, DAPS, DUPS, APC, UPC lipids (lipids where both the tails have more than two "D" type beads), while the FS class includes SM lipids (DPSM, DBSM, DXSM), glycolipids (DPG1, DXG1, DPG3, DXG3), ceramides (DPCE, DXCE), and LPC lipids (PPC).

Thickness, Curvature, and Lipid Composition. Membrane deformations were analyzed in terms of thickness and curvature. The method employed uses three interpolated grid-surfaces (upper, middle, and lower) from which thickness and curvature can be calculated. Surface averages are calculated for the last 5 μs on 30 μs long simulations, with a total of 2500 frames obtained by saving configurations every 2 ns.

The three surfaces are defined using different lipid beads: PO4 and GM1 beads for the upper surface (plane); the last bead of each lipid tail for the middle surface; the PO4 beads for the lower surface. For the definition of these surfaces lipid species that do flip-flop during the simulations (CHOL, DAG, and CER lipids [2]) were not taken into account. The choice of the GM1 bead for glycolipids was made with the help of small reference simulations (data not shown) consisting of binary mixtures of lipids (DPSM/DPG1) with equivalent acyl-chains and only differing in the headgroups. The GM4/GM1 beads of DPG1 have density peaks at positions equivalent to the DPSM-PO4 counterpart.

The method (to be published) has been implemented in C language, and has been derived from the numerical scheme described on a previous work that used MATLAB scripts,[9] and where gradients of surfaces are defined by interpolation on squared grids with a previous averaging on molecular coordinates carried out by a Gaussian filter, used to eliminate noise and generate smooth surfaces. The grid spacing used was 0.3 nm, with a Gaussian filter that averages data for a maximum of 6 cells radii for every point on the grids.

Leaflet thickness was calculated via middle surface to upper/lower surface distance for every point in the grids. The overall thickness was likewise calculated as distance between the upper and lower surfaces.

The same surfaces defined for thickness calculation are used for the curvature analysis. The estimated spontaneous curvature of a grid patch is equivalent to the average curvature of the lipids in the upper surface, minus the average spontaneous curvature of the lipids in the lower surface, taking the lipid local normals to the membrane as a reference. Consequently, the curvature for the lower leaflet would have to be multiplied by minus one in order to find the correlation between membrane curvature and spontaneous curvature only for the lower leaflet. Thickness values are given in nm, while mean and Gaussian curvatures are expressed on inverse distance units (nm^{-1} ad nm^{-2}, respectively).

Lipid composition is calculated by averaging the occupancy of cells for the entire set of 2500 frames, with units of lipid-tails per nm^2. These values are then changed into density units of mass per unit of area by including lipid masses. The first tails defining the beginning of the acyl-chain on all lipids were used as criteria to decide the occupancy on every frame of the set of lipids selected. The analysis was carried out for the CHOL, FS, PU and Others lipid classes. For each

class, the lipid composition was first calculated in terms of lipid density, and then changed into enrichment levels (Z_{new}) with respect to the average of the set (Z_{ave}). The new score, in percentage units, is defined by:

$$Z_{new} = \left(\frac{Z_{[i,j]}}{Z_{ave}} - 1\right) 100\%$$

where the indices [*i*,*j*] correspond to every point in the grid to be reweighted. The new score has the particularity to be positive for $Z_{i,j}$ values larger than Z_{ave}, and negative for values smaller than Z_{ave}. The 100% factor simply expresses the score as percentage units, indicating enrichment/depletion with respect to a homogeneous mixture with Z_{ave} score.

Depletion-enrichment index. The depletion-enrichment (D-E) index of a given lipid type was calculated for three distance cut-offs from the proteins, at 0.7, 1.4 and 2.1 nm. For a generic lipid type *L*, we first defined the ration of lipid *L* within a given cut-off *x* (namely $Ratio(L)_x$), and the ratio of the lipid *L* with respect to bulk (namely $Ratio(L)_{bulk}$) as follow:

$$Ratio(L)_x = \frac{(no.L)_x}{(tot.no.lipids)_x}$$

$$Ratio(L)_{bulk} = \frac{tot.no.(L)}{tot.no.lipids}$$

The enrichment of the lipid *L* for a given cut-off *x* is then calculated from the following ratio:

$$Enrichment(L) = \frac{Ratio(L)_x}{Ratio(L)_{bulk}}$$

Selected beads were used to calculate the number of lipids within a cut-off *x* from any bead of the protein: the ROH bead was chosen for cholesterol, while GL1 or AM1 beads were used for all the other lipid types.

For all the systems, the enrichment was calculated for the last 5 μs for each individual lipid type for the upper and lower leaflet separately. For cholesterol, DAGs (PODG, PIDG, PADG, PUDG) and CERs (DPCE, DXCE, PNCE, XNCE), the analysis was performed by combining the two leaflets together, due to the possible flip-flop of these lipid species. The enrichment was also calculated for groups of lipids categorized based on their headgroups (PC, PE, PS, PA, DAG, LPC, SM, CER, PI, PIPs, GM) or tails (FS, PU, CHOL and Others). In this case, the enrichment was calculated by combining the two leaflets together.

The final values shown in Figure 2A and Tables S1-S5 correspond to the average values obtained from the enrichment values of the four protein copies. Standard deviations are also reported.

The statistical significance of the D-E index was evaluated via a single sample T-test, according to the formula:

$$t = \frac{DE - 1}{SE}$$

where DE is the average D-E index calculated for a given lipid type (lipids grouped based on head group type or tail) within the chosen cut-off (0.7, 1.4, 2.1 nm); 1 is the null hypothesis, indicating that there is no enrichment or depletion of the chosen lipid type due to the proteins (based on our definition of the D-E index value this value is 1); SE, standard error, from a

population of 4 copies of each protein. We report the p-values, calculated from a two-tailed distribution and evaluated with a confidence level of 0.05 (Tables S6-S9).

Lipid count. The number of PC, GM, PE, and PIP lipids in contact with the proteins, as a function of time, was approximated by the number of PO4 (for PC, PE,), GM1 (for GM lipids) and CP (for PIP lipids) beads found within a 0.7 nm cut-off from the protein, as done similarly in previously published studies (Figures S7-S8).[10,11] The calculation was performed using the g_select tool implemented in GROMACS.[4]

Detailed discussion on GM and PIP lipids interactions with the proteins. GM-protein interactions are involved in a number of cellular functions, as GM-enriched domains participate to signal transduction and contribute to protein localization in the membrane.[12,13] In our simulations, GM aggregation around the proteins is detected for all the systems. There is, however, limited experimental data available on specific GM-protein interactions that could be used to validate the results, and the interactions between the large lipid polar group and the proteins might also be over-estimated by the force field.[14] GM-GM interactions as well as GM-protein interactions have been extensively studied with both atomistic and CG simulations.[15-22] While some of these studies used simplified membrane mixtures to study GM-protein interactions, here we show the ability of CG simulations to retrieve such interactions in the context of a more complex plasma membrane mixture. These lipid-sorting events appear linked to the presence of membrane proteins, and may be in line with the lateral compartmentalization of the membrane, i.e. the GM-enriched lipid raft hypothesis for protein localization and recruitment.[23] However, we did not observe large-scale lipid sorting phenomena in our simulations, as GM segregation lasting over tens of μs occurred only in close proximity of the proteins. While working on our set of simulations, due to the striking results on the protein-GM interactions, we tested further the reliability of such interactions.[14] Although the simulation conditions and parameters can have strong impacts on lipid-lipid interactions, the effects on lipid-protein interactions are not easy to interpret,[14] and our control simulations here show that for AQP1 the observed GM clustering is not sensitive to the simulation conditions, and in particular to the type of water model in use.

In the lower leaflet, the membrane components that behave most similarly to the GM lipids of the upper leaflet are PIP lipids. Indeed, PIP lipids form small clusters in lipid bilayers and interact or bind with membrane proteins in many simulation studies.[2,17,20,21] Here, common to most of the systems is a clear PIP lipids enrichment, which persists over few lipids shells around the proteins. The strength of electrostatic interactions between lipids and proteins might be biased by the use of the standard water model, here applied to all the simulation systems. However, the control simulation on AQP1 revealed a significant enrichment of PIP lipids even with the polarizable water model.[24] Moreover, direct interaction between PIP lipids and membrane proteins has been shown for a number of channels and receptors, including EGFR and DAT, which are among the systems we simulated.[25-27] Given the variety of roles of this lipid type in the plasma membrane, from peripheral proteins localization, signaling, membrane trafficking and membrane protein function regulation,[28,29] it is not surprising that the simulations detect interactions between PIP lipids and many other membrane proteins, thus providing new details on possible specific lipid-protein interactions to investigate further.

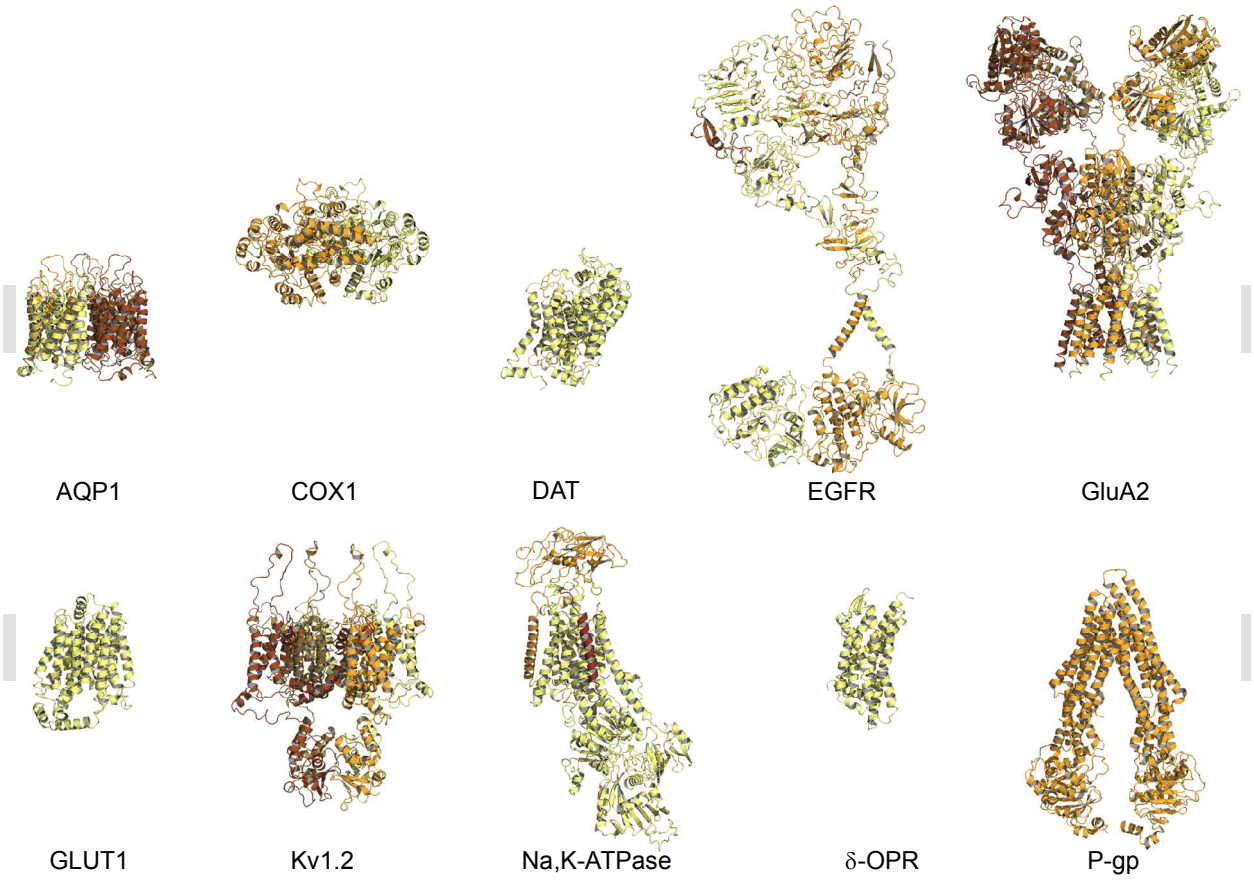

Figure S1. Membrane Proteins. Atomistic structures of the membrane proteins selected for this study. Each protein is shown as cartoons, coloured from light yellow to brown when multiple chains are present. The gray-shaded area represents the hydrophobic region of the membrane.

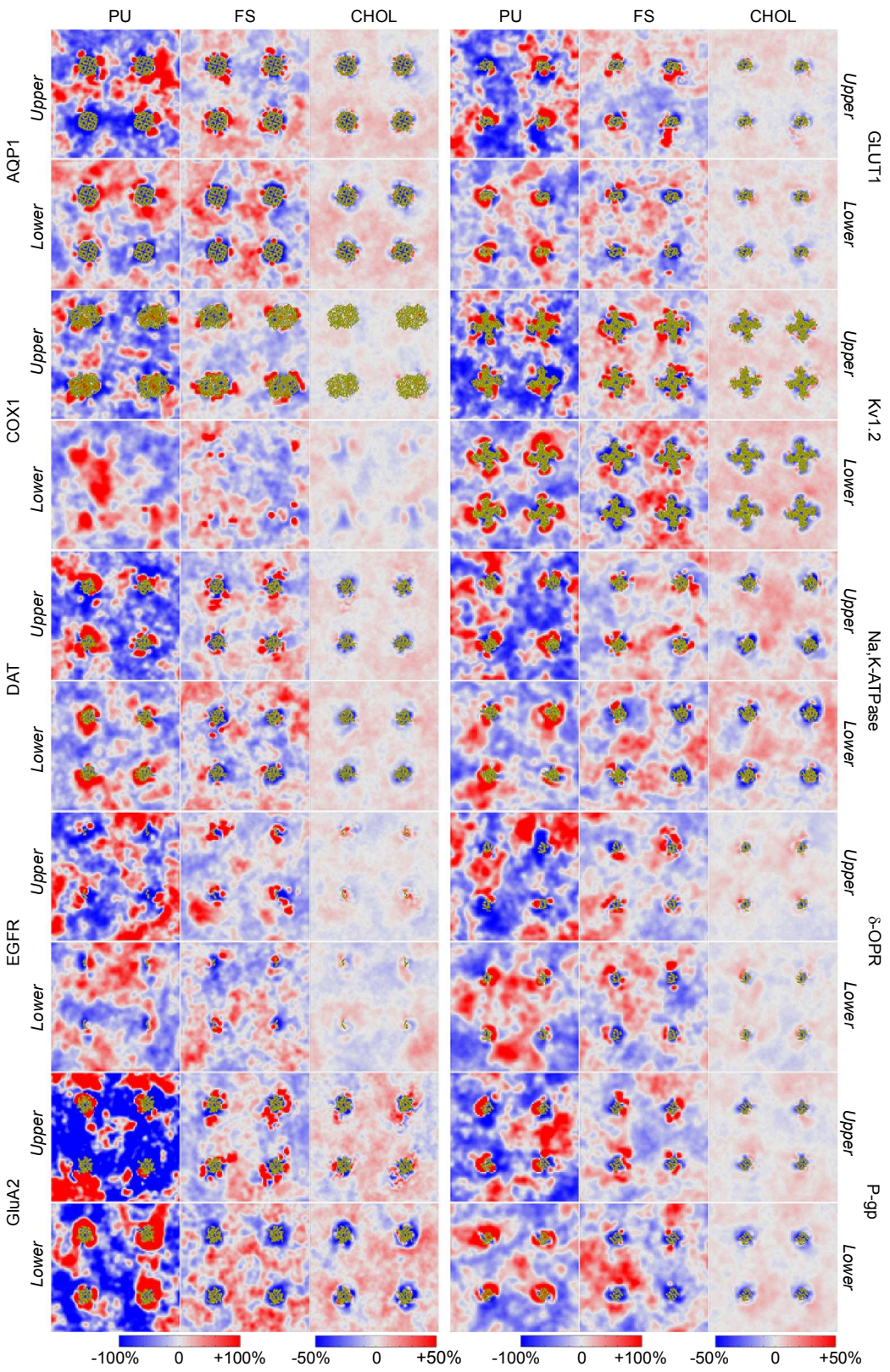

Figure S2. Lipid density maps. Lipid density analysis, for upper and lower leaflet, of the poly-unsaturated (PU), fully-saturated (FS), and cholesterol (CHOL) classes. The lipid density is

represented by x and y 2D maps, averaged between 25 to 30 μs. The maps are colored by relative enrichment (red) or depletion (blue), calculated with respect to the average (white) density of a given class. The portion of the protein intersecting the upper and lower surfaces used for the calculation is shown in yellow ribbons.

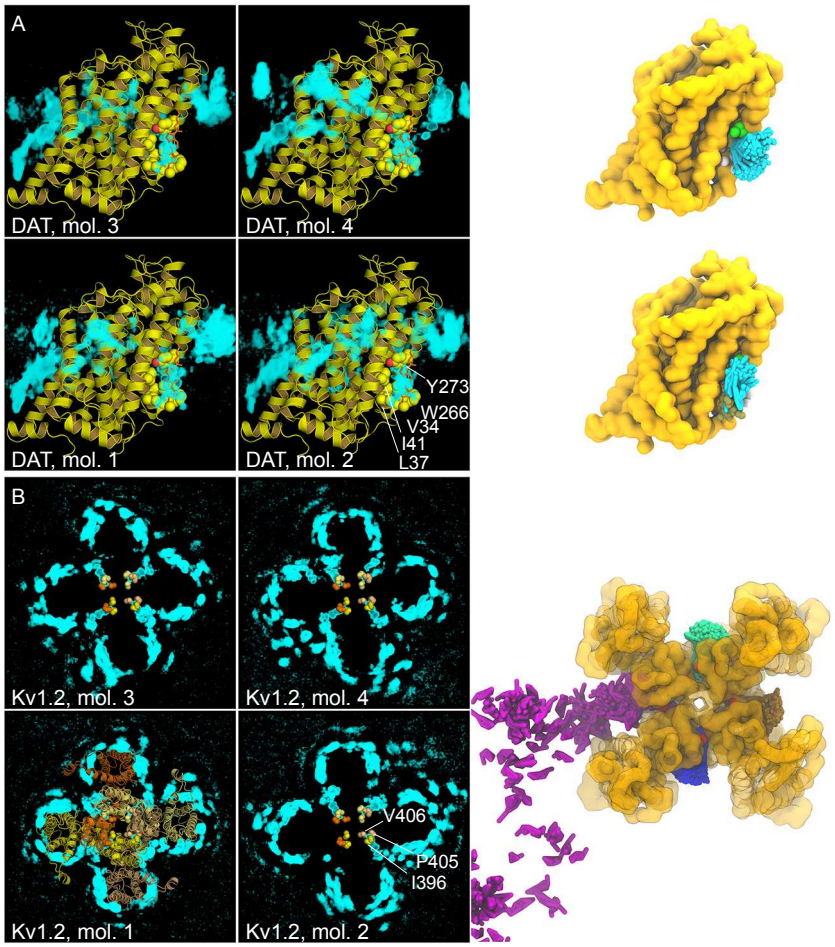

Figure S3. Specific CHOL binding sites in DAT and Kv1.2. (A) The panel on the left shows the lateral view of cholesterol number density (in cyan) for each of the four DAT molecules of the system. The protein shown corresponds to the atomistic crystal structure used in the simulation, superimposed to its CG model after aligning the BB beads to the α-carbons. The bound cholesterol is shown as orange sticks, while the side-chains of nearby residues are shown as spheres. On the right are two examples of possible CHOL binding modes (cyan sticks, with tan ROH beads) near its crystallographic binding site. As a reference, the side-chains of Y273 and L37 are shown in green and white spheres, respectively. (B) The panel on the left shows the cholesterol number density (in cyan) for each of the four Kv1.2 molecules of the system (the initial atomistic structure is shown), seen from the extracellular side. The monomers of each tetramer are shown in yellow, orange, pale yellow and sand cartoons, while the side-chains of some of the residues lining the CHOL binding site are shown as spheres. The panel on the right

shows one of the tetramers (transparent yellow surface), with four cholesterol molecules (in yellow, brown, green and magenta sticks) bound. Each cholesterol molecule is shown every 2 ns, from 25 to 30 μs. As a reference, the side-chain of I396 is shown in red spheres. In (A-B) the number density was calculated in proximity of each protein molecules for the last 5 μs of the simulation, as described in Mehmood et al.[11] All the voxels with a density value that is above 99% of the maximum observed density value are displayed as volume maps with PyMOL (Schrodinger, L., 2015, The PyMOL Molecular Graphics System, Version 1.8).

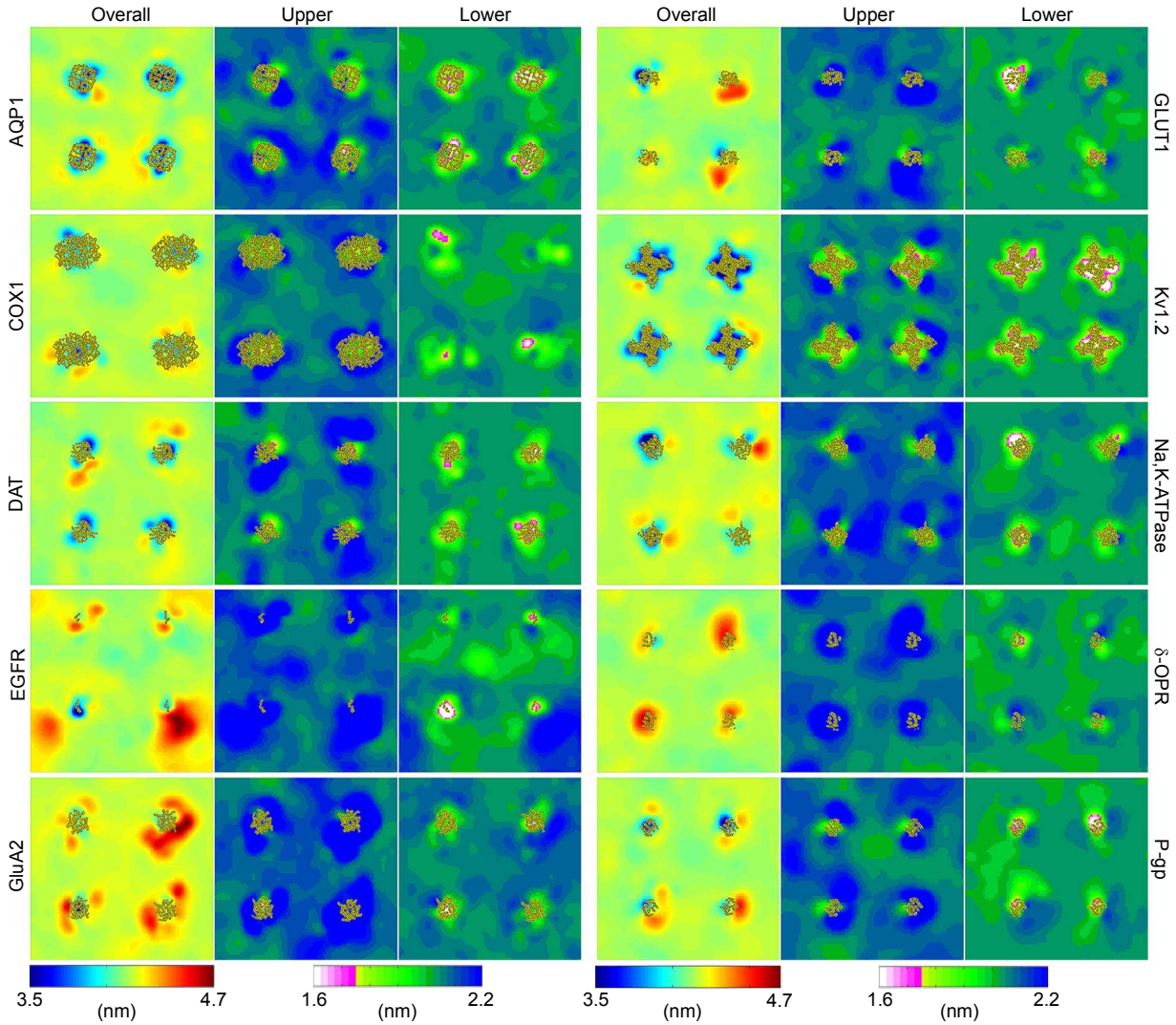

Figure S4. Membrane thickness. For each of the simulation systems, membrane thickness is shown as x and y 2D maps, averaged between 25 to 30 μs. Upper, middle and lower surfaces were defined by PO4 and GM1 beads (upper), last bead of each lipid tail (middle), and PO4 and CP beads (lower), respectively. Overall thickness, i.e. the distance calculated between the upper and lower surfaces, is shown color-coded according to a 3.5 to 4.7 nm range. Over the systems, the 2D maps highlight a complex thickness landscape, with islands of higher or lower thickness, often localized and confined near the proteins. The thickness for the upper leaflet (as distance between the upper and the middle surface) and for the lower leaflet (as distance between the lower and the middle surface) is shown on a different color scale, ranging from 1.6 to 2.2 nm. The position of the four protein copies in each simulation box is indicated by representing the proteins in yellow ribbons.

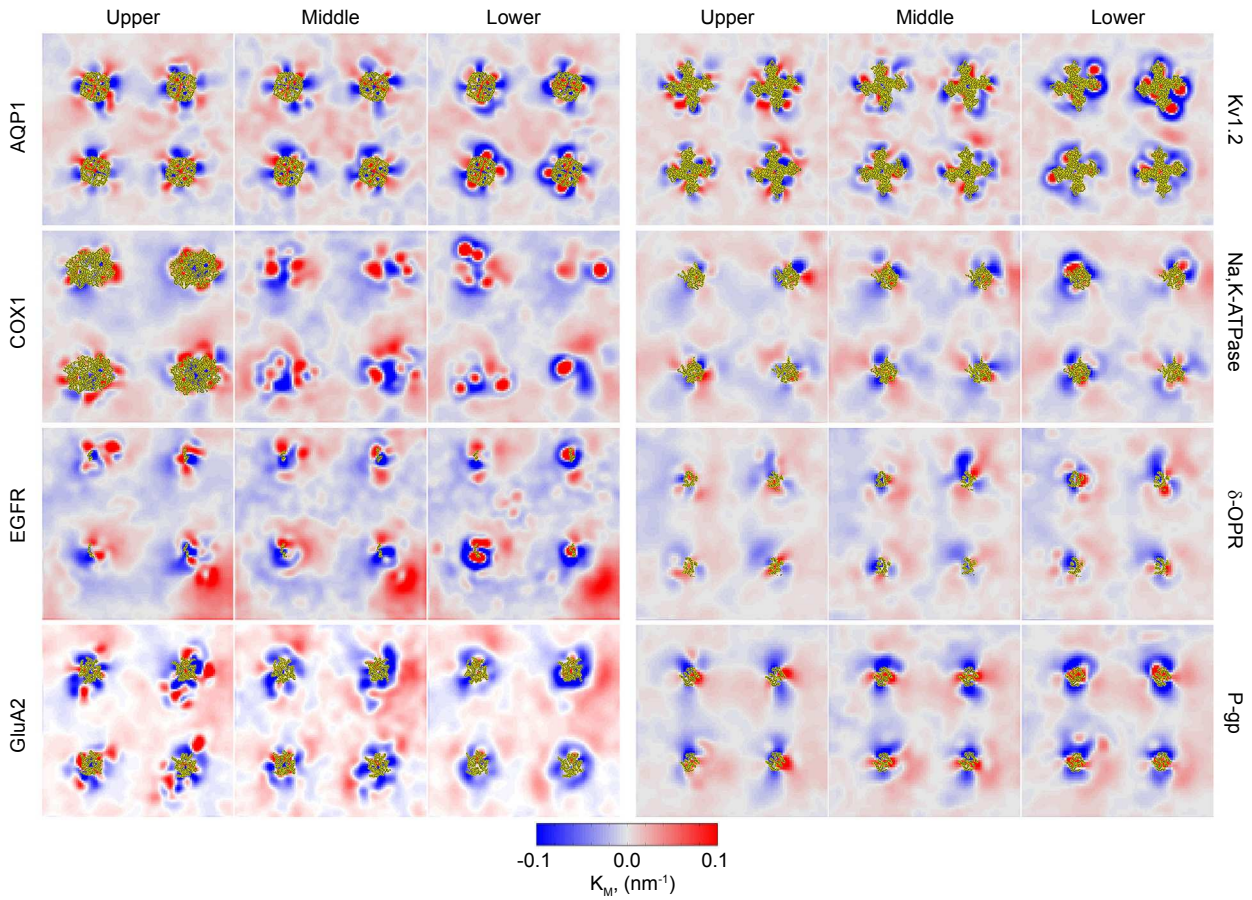

Figure S5. Mean curvature (K_M) maps. 2D maps of K_M calculated for each simulation system, and averaged between 25 to 30 μs. The upper, middle and lower surfaces used to calculated thickness were employed to derive the values of K_M, defined with respect to the normal of the upper surface. Stronger negative (blue) and positive (red) values are found in the immediate proximity of each protein, occasionally extending to the neighbors molecules, as, for example, in the case of P-gp. The position of the four proteins in each simulation box is indicated by representing the proteins in yellow ribbons. DAT and GLUT1 were excluded from this analysis as these systems were simulated in the presence of position restraints on the PO4 beads.

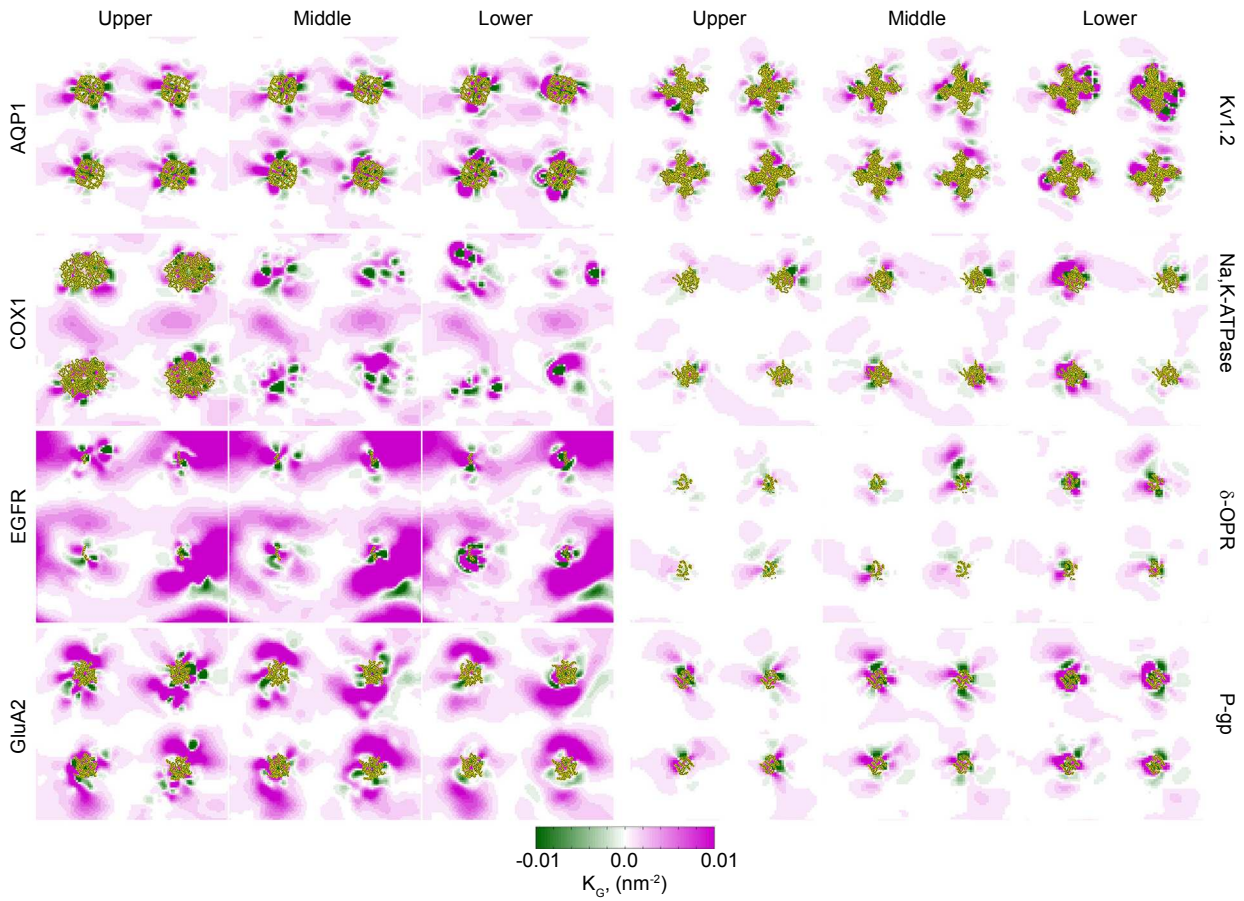

Figure S6. Gaussian curvature (K_G) maps. 2D maps of the K_G calculated for each simulation system and averaged over the simulation from 25 to 30 μs. K_G was calculated for the same surfaces used for K_M. Saddles (negative K_G, magenta) and convex/concave regions of the membrane (positive K_G, green) are often found near the proteins. For AQP1, COX1, EGFR, and GluA2 saddled regions spread greatly over the simulation box. The position of the four proteins in each simulation box is indicated by representing the proteins in yellow ribbons. DAT and GLUT1 were excluded from this analysis as these systems were simulated in the presence of position restraints on the PO4 beads.

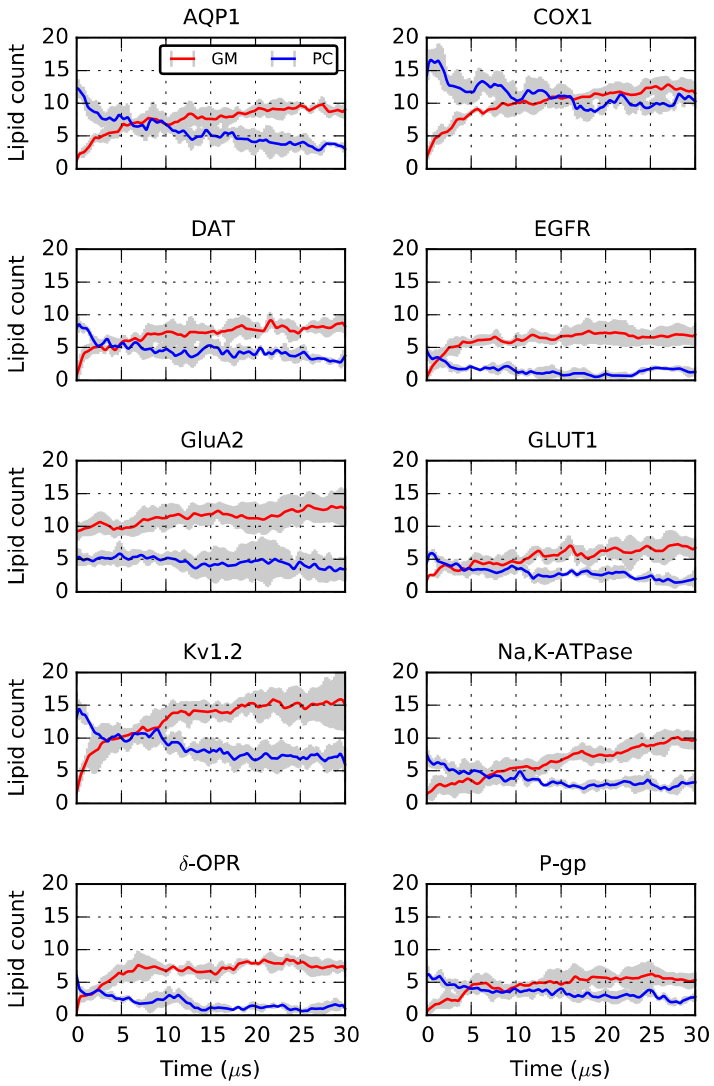

Figure S7. Lipid count for PC and GM lipids in the upper leaflet. Number of upper leaflet PC (blue) and GM (red) lipids that as a function of time are found within 0.7 nm cutoff from the proteins. The lipid count was calculated based on the number of PO4 beads (for PE lipids) or GM1 beads (for GM lipids) that satisfy the cutoff. Plotted are the running averages calculated from the four protein molecules in each system, over windows of 1 μs. Standard deviation is shown in gray.

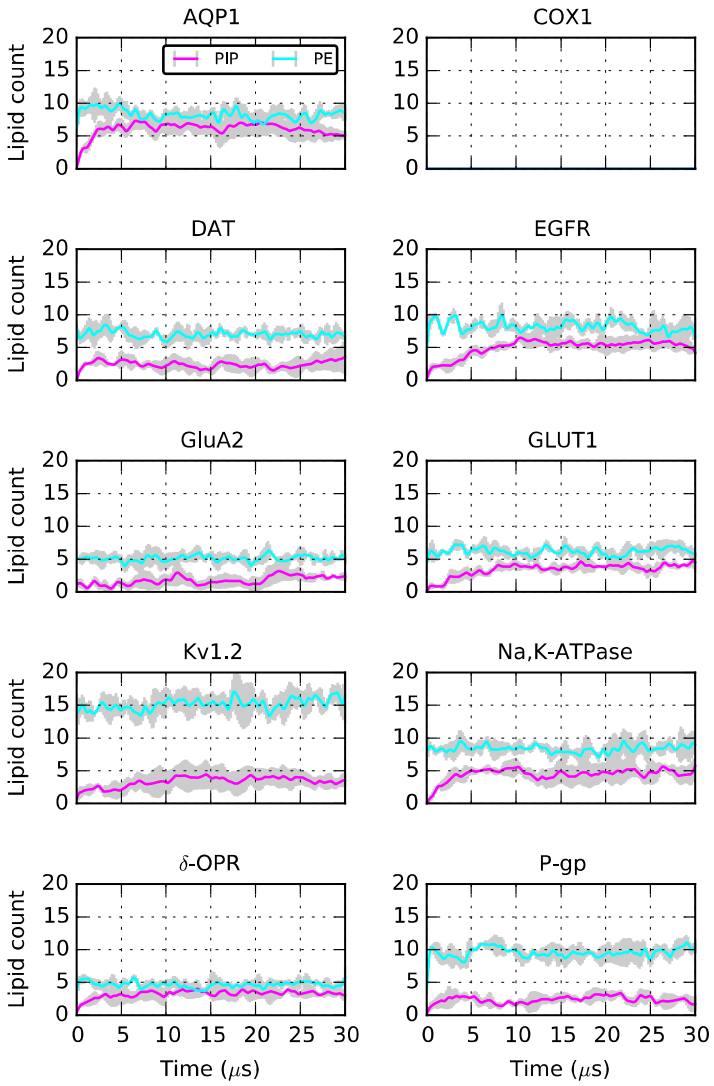

Figure S8. Lipid count for PE and PIP lipids in the lower leaflet. Number of lower leaflet PE (cyan) and PIP (magenta) lipids that as a function of time are found within 0.7 nm cutoff from the proteins. The lipid count was calculated based on the number of PO4 beads (for PE lipids) and CP beads (for PIP lipids) that satisfy the cutoff. Plotted are the running averages calculated from the four protein molecules in each system, over windows of 1 μs. Standard deviation is shown in gray. For COX1, embedded only partially in the upper leaflet, no PE or PIP lipids were detected within the chosen cutoff.

REFERENCES

(1) Lomize, M. A.; Lomize, A. L.; Pogozheva, I. D.; Mosberg, H. I. OPM: orientations of proteins in membranes database. *Bioinformatics* **2006,** *22*, 623-625.

(2) Ingolfsson, H. I.; Melo, M. N.; van Eerden, F. J.; Arnarez, C.; Lopez, C. A.; Wassenaar, T. A.; Periole, X.; de Vries, A. H.; Tieleman, D. P.; Marrink, S. J. Lipid organization of the plasma membrane. *J. Am. Chem. Soc.* **2014,** *136*, 14554-14559.

(3) Wassenaar, T. A.; Ingolfsson, H. I.; Bockmann, R. A.; Tieleman, D. P.; Marrink, S. J. Computational lipidomics with insane: a versatile tool for generating custom membranes for molecular simulations. *J. Chem. Theory Comput.* **2015,** *11*, 2144-2155.

(4) Hess, B.; Kutzner, C.; van der Spoel, D.; Lindahl, E. GROMACS 4: Algorithms for highly efficient, load-balanced, and scalable molecular simulation. *J. Chem. Theory Comput.* **2008,** *4*, 435-447.

(5) de Jong, D. H.; Singh, G.; Bennett, W. F.; Arnarez, C.; Wassenaar, T. A.; Schafer, L. V.; Periole, X.; Tieleman, D. P.; Marrink, S. J. Improved parameters for the Martini coarse-grained protein force field. *J. Chem. Theory Comput.* **2013,** *9*, 687-697.

(6) Bussi, G.; Donadio, D.; Parrinello, M. Canonical sampling through velocity rescaling. *J. Chem. Phys.* **2007,** *126*, 014101.

(7) Berendsen, H. J. C.; Postma, J. P. M.; Vangunsteren, W. F.; Dinola, A.; Haak, J. R. Molecular-Dynamics with Coupling to an External Bath. *J. Chem. Phys.* **1984,** *81*, 3684-3690.

(8) Yesylevskyy, S. O.; Schafer, L. V.; Sengupta, D.; Marrink, S. J. Polarizable water model for the coarse-grained MARTINI force field. *PLoS Comput. Biol.* **2010,** *6*, e1000810.

(9) Mendez-Villuendas, E.; Baoukina, S.; Tieleman, D. P. Challenges in analysing and visualizing large-scale molecular dynamics simulations: domain and defect formation in lung surfactant monolayers. *J. Phys. Conf. Ser.* **2012,** *385*, 012002.

(10) Kalli, A. C.; Sansom, M. S.; Reithmeier, R. A. Molecular dynamics simulations of the bacterial UraA H+-uracil symporter in lipid bilayers reveal a closed state and a selective interaction with cardiolipin. *PLoS Comput. Biol.* **2015,** *11*, e1004123.

(11) Mehmood, S.; Corradi, V.; Choudhury, H. G.; Hussain, R.; Becker, P.; Axford, D.; Zirah, S.; Rebuffat, S.; Tieleman, D. P.; Robinson, C. V.et al. Structural and functional basis for lipid synergy on the activity of the antibacterial peptide ABC transporter McjD. *J. Biol. Chem.* **2016,** *291*, 21656-21668.

(12) Hakomori Si, S. I. The glycosynapse. *Proc. Natl. Acad. Sci. U. S. A.* **2002,** *99*, 225-232.

(13) Masserini, M.; Pitto, M.; Ferraretto, A.; Brunne, J.; Palestini, P. Glycolipid-protein interaction in the mechanism of signal transduction: studies with a photoactivable ganglioside analogue. *Acta Biochim. Pol.* **1998,** *45*, 393-401.

(14) Gu, R. X.; Ingolfsson, H. I.; de Vries, A. H.; Marrink, S. J.; Tieleman, D. P. Ganglioside-lipid and ganglioside-protein interactions revealed by coarse-grained and atomistic molecular dynamics simulations. *J. Phys. Chem. B* **2016,** *121*, 3262-3275.

(15) Manna, M.; Rog, T.; Vattulainen, I. The challenges of understanding glycolipid functions: An open outlook based on molecular simulations. *BBA-Mol. Cell. Biol. L.* **2014,** *1841*, 1130-1145.

(16) de Jong, D. H.; Lopez, C. A.; Marrink, S. J. Molecular view on protein sorting into liquid-ordered membrane domains mediated by gangliosides and lipid anchors. *Faraday Discuss.* **2013,** *161*, 347-363; discussion 419-359.

(17) Koldso, H.; Shorthouse, D.; Helie, J.; Sansom, M. S. P. Lipid clustering correlates with membrane curvature as revealed by molecular simulations of complex lipid bilayers. *PLoS Comput. Biol.* **2014,** *10*, e1003911.

(18) Lopez, C. A.; Sovova, Z.; van Eerden, F. J.; de Vries, A. H.; Marrink, S. J. Martini Force Field Parameters for Glycolipids. *J. Chem. Theory Comput.* **2013,** *9*, 1694-1708.

(19) Shorthouse, D.; Hedger, G.; Koldso, H.; Sansom, M. S. Molecular simulations of glycolipids: Towards mammalian cell membrane models. *Biochimie* **2016,** *120*, 105-109.

(20) Marino, K. A.; Prada-Gracia, D.; Provasi, D.; Filizola, M. Impact of lipid composition and receptor conformation on the spatio-temporal organization of mu-opioid receptors in a multi-component plasma membrane model. *PLoS Comput. Biol.* **2016,** *12*, e1005240.

(21) Koldso, H.; Sansom, M. S. P. Organization and dynamics of receptor proteins in a plasma membrane. *J. Am. Chem. Soc.* **2015,** *137*, 14694-14704.

(22) Hedger, G.; Shorthouse, D.; Koldso, H.; Sansom, M. S. Free energy landscape of lipid interactions with regulatory binding sites on the transmembrane domain of the EGF receptor. *J. Phys. Chem. B* **2016,** *120*, 8154-8163.
(23) Lingwood, D.; Simons, K. Lipid rafts as a membrane-organizing principle. *Science* **2010,** *327*, 46-50.
(24) Yesylevskyy, S. O.; Schafer, L. V.; Sengupta, D.; Marrink, S. J. Polarizable water model for the coarse-grained MARTINI force field. *PLoS Comput. Biol.* **2010,** *6*, e1000810.
(25) Hamilton, P. J.; Belovich, A. N.; Khelashvili, G.; Saunders, C.; Erreger, K.; Javitch, J. A.; Sitte, H. H.; Weinstein, H.; Matthies, H. J. G.; Galli, A. PIP2 regulates psychostimulant behaviors through its interaction with a membrane protein. *Nat. Chem. Biol.* **2014,** *10*, 582-589.
(26) Michailidis, I. E.; Rusinova, R.; Georgakopoulos, A.; Chen, Y. B.; Iyengar, R.; Robakis, N. K.; Logothetis, D. E.; Baki, L. Phosphatidylinositol-4,5-bisphosphate regulates epidermal growth factor receptor activation. *Pflugers Arch. - Eur. J. Phy.* **2011,** *461*, 387-397.
(27) Wang, Y.; Gao, J.; Guo, X. D.; Tong, T.; Shi, X. S.; Li, L. Y.; Qi, M.; Wang, Y. J.; Cai, M. J.; Jiang, J. G.et al. Regulation of EGFR nanocluster formation by ionic protein-lipid interaction. *Cell Res.* **2014,** *24*, 959-976.
(28) Logothetis, D. E.; Petrou, V. I.; Zhang, M.; Mahajan, R.; Meng, X. Y.; Adney, S. K.; Cui, M.; Baki, L. Phosphoinositide control of membrane protein function: a frontier led by studies on ion channels. *Annu. Rev. Physiol.* **2015,** *77*, 81-104.
(29) Raiborg, C.; Wenzel, E. M.; Pedersen, N. M.; Stenmark, H. Phosphoinositides in membrane contact sites. *Biochem. Soc. Trans.* **2016,** *44*, 425-430.